RESEARCH ARTICLE

Key Points:
- At the Doi Inthanon neutron monitor (NM), we operated a calibration (Cal) NM
- We directly measured the Cal/NM count rate ratio dependence on surroundings
- Monte Carlo Cal/NM results match data to a few percent for different Cal locations

Correspondence to:
D. Ruffolo,
david.ruf@mahidol.ac.th

Measurement and simulation of neutron monitor count rate dependence on surrounding structure

N. Aiemsa-ad[1,2,3], D. Ruffolo[3,4], A. Sáiz[3,4], P.-S. Mangeard[4,5], T. Nutaro[3,6], W. Nuntiyakul[3,4,7], N. Kamyan[4], T. Khumlumlert[1], H. Krüger[8], H. Moraal[8], J. W. Bieber[9], J. Clem[9], and P. Evenson[9]

[1]Department of Physics, Faculty of Science, Naresuan University, Phitsanulok, Thailand, [2]Faculty of Science and Technology, Rajabhat Rajanagarindra University, Chachoengsao, Thailand, [3]Thailand Center of Excellence in Physics, CHE, Ministry of Education, Bangkok, Thailand, [4]Department of Physics, Faculty of Science, Mahidol University, Bangkok, Thailand, [5]National Astronomical Research Institute of Thailand, Chiang Mai, Thailand, [6]Department of Physics, Faculty of Science, Ubon Ratchathani University, Ubon Ratchathani, Thailand, [7]Faculty of Science, Chandrakasem Rajabhat University, Bangkok, Thailand, [8]Centre for Space Research, School of Physical and Chemical Sciences, North-West University, Potchefstroom, South Africa, [9]Bartol Research Institute, Department of Physics and Astronomy, University of Delaware, Newark, Delaware, USA

Abstract Neutron monitors are the premier instruments for precise measurements of time variations (e.g., of solar origin) in the galactic cosmic ray (GCR) flux in the range of ~1–100 GeV. However, it has proven challenging to accurately determine the yield function (effective area) versus rigidity in order to relate a neutron monitor's count rate with those of other monitors worldwide and the underlying GCR spectrum. Monte Carlo simulations of the yield function have been developed, but there have been few opportunities to validate these observationally, especially regarding the particular environment surrounding each monitor. Here we have precisely measured the count rate of a calibration neutron monitor near the Princess Sirindhorn Neutron Monitor (PSNM) at Doi Inthanon, Thailand (18.59°N, 98.49°E, 2560 m altitude), which provides a basis for comparison with count rates of other neutron monitors worldwide that are similarly calibrated. We directly measured the effect of surrounding structure by operating the calibrator outside and inside the building. Using Monte Carlo simulations, we clarify differences in response of the calibrator and PSNM, as well as the calibrator outside and inside the building. The dependence of the calibrator count rate on surrounding structure can be attributed to its sensitivity to neutrons of 0.5–10 MeV and a shift of sensitivity to nucleons of higher energy when placed inside the building. Simulated calibrator to PSNM count rate ratios inside and outside agree with observations within a few percent, providing useful validation and improving confidence in our ability to model the yield function for a neutron monitor station.

1. Introduction

A neutron monitor is a standard ground-based instrument for measuring time variations in the flux of galactic cosmic rays (GCRs) by detecting secondary particles (mostly neutrons) from their atmospheric showers. Ground-based measurements of GCR flux variations over 22 year solar magnetic cycles, 11 year sunspot cycles, and the Sun's 27 day rotation period, as well as the GCR anisotropy from diurnal count rate variations over the Earth's 1 day rotation period, provide unique and important information about the state of the heliosphere [*Okazaki et al.*, 2008; *Yeeram et al.*, 2014; *Nuntiyakul et al.*, 2014]. Cosmic rays can reach a given location on Earth only if their rigidity (related to momentum per charge) exceeds the local geomagnetic cutoff rigidity. Simultaneous measurements from neutron monitor stations worldwide could in principle be combined to determine the GCR spectrum over a rigidity range of 1 to 17 GV. This could be done continuously, which would improve the interpretation of GCR flux variations. Directly combining the count rates from different neutron monitors to track spectral changes requires an accurate intercalibration between the stations to within ~0.2% [*Moraal et al.*, 2000]. From a modeling perspective, substantial progress has been made toward determining the yield function (effective area) of neutron monitors by fitting data [e.g., *Caballero-Lopez and Moraal*, 2012] and from Monte Carlo simulation [e.g., *Clem and Dorman*, 2000; *Mishev et al.*, 2013]. Further effort is needed to systematically study the effect of the electronic dead time as a key parameter for precise measurements. There is also some uncertainty in the local interstellar spectrum [*Herbst et al.*, 2010] and effects of the choice of Monte Carlo simulation package, treatment of alpha particles and heavy ions, and the exclusion of certain secondary particles [*Mishev and Velinov*, 2014]. Furthermore, the effects of local surroundings and atmospheric structure
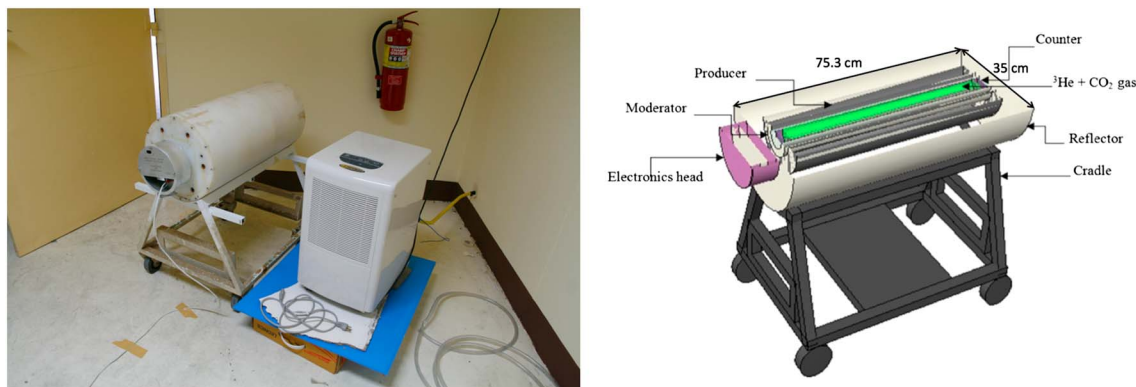
Figure 1. (left) Photograph of a calibration neutron monitor ("calibrator") inside the Princess Sirindhorn Neutron Monitor (PSNM) building at Doi Inthanon, Thailand. A dehumidifier is to the right of the calibrator. (right) Schematic cross section of the calibrator. Most counts are due to atmospheric neutrons that interact in the producer (made of lead rings), generating several more neutrons that can be detected by the ^{3}He gas proportional counter tube.

require detailed study for each location. While much interesting science can be done without precise knowledge of the yield function [*Grieder*, 2001], a neutron monitor will become a more powerful instrument when its yield function is fully understood and data from the worldwide network of neutron monitors can be combined to precisely track the GCR spectrum. Combining data from neutron monitors at various cutoff rigidities can also be useful in the analyses of relativistic solar particle events [*Cramp et al.*, 1997; *Vashenyuk et al.*, 2006].

In the present work, we report on two advances toward these goals obtained from a relatively portable calibration neutron monitor (hereafter, "the calibrator") [*Krüger et al.*, 2008], shown in Figure 1, in conjunction with the *Princess Sirindhorn Neutron Monitor* (PSNM) at the summit of Doi Inthanon, Thailand's highest mountain (18.59°N, 98.49°E, 2560 m altitude). The PSNM, an 18-tube NM64 neutron monitor or "18NM64," operates at the world's highest geomagnetic cutoff rigidity for a fixed station (16.8 GV vertical cutoff), and is therefore of particular importance to anchor the high end of the GCR spectrum as inferred from neutron monitor data. The measurements reported here relate the PSNM count rate to that of the calibrator, in turn relating its station-specific count rate to other stations around the world, including SANAE, Hermanus, Potchefstroom, and Kiel [*Moraal et al.*, 2003; *Krüger and Moraal*, 2010], and others that may be calibrated in the future.

While a calibration at one epoch is useful, there is some uncertainty in how the calibration changes with GCR spectral variations, and in particular with solar cycle-dependent effects ("solar modulation") on the GCR spectrum. Thus, the ultimate solution for how to interpret neutron monitor count rates is to accurately model their yield functions using Monte Carlo simulations of cosmic ray interactions in Earth's atmosphere producing atmospheric secondary cosmic rays and interactions of these secondary particles in the neutron monitor and its surrounding building or structure. Such simulations have been performed previously [e.g., *Clem and Dorman*, 2000; *Mishev et al.*, 2013], but there have been few opportunities to validate such simulations. The calibrator provided us with a special opportunity to validate modeling of secondary cosmic ray interactions at the PSNM station through extended calibration runs with the calibrator both outside and inside the PSNM building, collecting 9.1×10^6 and 4.5×10^6 counts in the calibrator, respectively. Our simulation results for the ratio of count rates of the calibrator and PSNM, hereafter called the "Cal/NM" ratio, are in agreement with these precise measurements to within a few percent, providing a validation of our modeling techniques and giving us confidence that count rate variations at fixed neutron monitor stations can be related to the underlying GCR spectral variations.

2. Detection Equipment and Observations

The calibrator used in this work is relatively compact, with a length of 753 mm and a mass of 223 kg (including the cradle) [*Krüger et al.*, 2003, 2008], allowing it to be transported to various locations around the world. Figure 1 shows a photograph of the calibrator during deployment inside the PSNM building at Doi Inthanon, Thailand, and also a cross-sectional illustration of the components inside. The innermost component of the calibrator is a LND25382 proportional counter tube (manufactured by LND, Inc.) of 51 mm diameter and 652 mm length filled with 4 atm of ^{3}He (97%) and CO_2 quench gas (3%), in which neutrons are detected
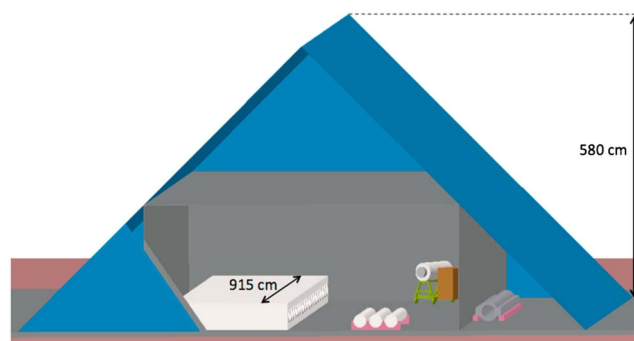
Figure 2. Illustration of the geometry for Monte Carlo simulations of the calibrator inside the PSNM building at Doi Inthanon, Thailand. This cutaway view removes most of the east wall. The calibrator (white cylinder at right) was operated inside the station during June 2010. The 18-tube NM64 neutron monitor (left) and three bare neutron counter tubes (front) have been operating there since 2007. Spare lead rings are kept in a storage room to the right.

by means of the reaction $^3\text{He}(n,p)^3\text{H}$. This is surrounded by a cylindrical polyethylene moderator of inner diameter 60.5 mm and outer diameter 99.5 mm. The lead producer comprises seven rings that together form a hollow cylinder of inner diameter 101 mm and outer diameter 193 mm, and mass 145 kg. Atmospheric secondary cosmic rays of various species interact in the lead to produce spallation neutrons that are then detected in the ^3He counter. (The detector response is predominantly due to sub-GeV atmospheric neutrons - see details below.) Finally, the outermost cylinder is a polyethylene reflector of inner diameter 194 mm and outer diameter 350 mm that serves to exclude some

neutrons in the MeV range or lower produced in the calibrator's surroundings and also helps contain neutrons from the lead producer. There are also caps of polyethylene reflector at each end, of 50 mm thickness and 350 mm diameter. At Doi Inthanon the typical calibrator count rate was ≈ 3.5 Hz.

The PSNM station, at the summit of Doi Inthanon, is located at geographic coordinates 18.59°N and 98.49°E, at an altitude of about 2560 m. Because the present work concerns the effect of surrounding structure on neutron monitor count rates, we describe various components of the PSNM station, as shown in Figure 2, and include them in the simulation geometry. The building has an area of 10×10 m^2 and two metal roof panels inclined at 45°. There are also inner vertical walls and a ceiling of concrete that define a smaller rectangular enclosure. The main neutron monitor contains 18 counter tubes in one continuous row, with the standard NM64 design [*Hatton and Carmichael*, 1964] that includes lead producer (29 t) and polyethylene moderator and reflector. A typical count rate is ≈ 34 Hz per tube. The building also houses three bare neutron counters, each with moderator but no producer or reflector, which are also visible in Figure 2 and count ≈ 6 Hz per tube. The count rates of tubes in the neutron monitor are higher than those of bare tubes, mainly because the lead producer can generate multiple neutrons from a single incident atmospheric secondary particle. Data from the three bares were not used for the present study.

Based on prior experience using the calibrator in other locations, it was suggested that the calibrator should be operated over a pool of water, which moderates neutrons, to provide a standard surface underneath, and in open atmosphere, far away from any structures that absorb or produce neutrons [*Krüger and Moraal*, 2010]. In practice, the latter requirement is expressed as a need to operate outdoors and avoid any obstructions higher than 20° above the horizon. Ideally, the calibrator then serves as an independent monitoring system whose count rate depends only on latitude, longitude, and atmospheric pressure and can calibrate a neutron monitor and its surrounding structure without the calibrator being affected by that structure. At Doi Inthanon, a site meeting these requirements was found on top of a concrete bunker a few meters high, located a few meters south of the PSNM building and down a rocky incline (Figure 3). This allowed a power cable and data cable to be connected to the building and the data acquisition computer within. A portable swimming pool with a wire framework and vinyl lining, provided with the calibrator, was set up and filled with water to the desired height. The calibrator cradle was placed on four concrete pillars in the center of the swimming pool, keeping the calibrator itself above the water level.

The calibrator was operated inside or near the PSNM station during November 2009 to June 2010. This time period corresponded to solar minimum conditions, and indeed, our observations started near the time of the highest cosmic ray rates ever recorded in the space age [*Mewaldt et al.*, 2010]. In the present work, we focus on the relative count rates of the calibrator and PSNM, i.e., the Cal/NM ratio.

The minimum requirement for the calibration is to acquire 10^6 counts, which required only about 4 days of data taking at our high-altitude location. Therefore, we also took the opportunity to measure the difference in
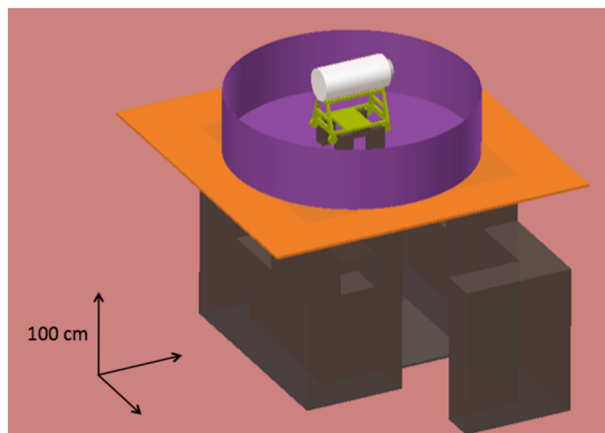
Figure 3. Illustration of the geometry for Monte Carlo simulations of the calibrator outside but nearby the PSNM building at Doi Inthanon, Thailand. It was set above a swimming pool on top of a bunker and operated for various water heights and calibrator heights during November 2009 to June 2010.

the count rate ratio for the calibrator outside or inside the building, and for different environmental conditions outside, where we varied the height of the calibrator (the underside of the reflector) above the bottom of the pool, which we call "calibrator height," and also varied the height of the water surface above the bottom of the pool, which we call the "water height." The calibrator height was always greater than the water height to keep the calibrator above the water. We operated in a total of 15 configurations, as summarized in Table 1, but there were technical difficulties with Configurations 7 and 14, so those are not included in the table, and those data were not analyzed.

An important component of the calibrator is the electronics head (including a cylindrical metal cover) attached directly to the front. In these observations, we employed three different sets of electronics. We used two different preamplifiers (attached to the counter tube) with an electronics head made at North-West University, South Africa, specifically for the calibrator. We refer to those two combinations of preamplifier and electronics head as the NWU1 and NWU2 electronics. We also used a remote electronics head made by the Bartol Research Institute, University of Delaware, USA, which we refer to as the BRI electronics. Table 1 specifies which electronics were used for each configuration.

Table 1. Observations With the Calibrator at Doi Inthanon[a]

Configuration	Calibrator Height (cm)	Water Height (cm)	Start Time[b]	Stop Time[b]	Electronics	Cal/NM[c]	N[d]
1	140	0	2009/327/11	2009/341/03	NWU1	0.005710(6)	2.97×10^6
2	140	50	2009/342/01	2009/349/03	NWU1	0.005635(6)	1.98×10^6
3	140	68	2009/349/08	2009/357/06	NWU1	0.005622(6)	2.11×10^6
4	140	25	2009/357/07	2009/362/02	NWU1	0.005659(7)	1.27×10^6
5	70	0	2009/362/08	2010/005/01	NWU1	0.005744(7)	2.17×10^6
6	70	60	2010/008/11	2010/017/04	NWU1	0.005505(5)	2.28×10^6
8	70	65	2010/042/07	2010/096/23	BRI	0.004860(2)	9.12×10^6
9	70	65	2010/098/08	2010/110/08	NWU1	0.005506(4)	2.68×10^6
10	70	65	2010/112/05	2010/127/05	NWU2	0.005637(6)	2.76×10^6
11	70	50	2010/127/06	2010/132/01	NWU2	0.005771(12)	8.99×10^5
12	70	25	2010/132/02	2010/155/02	NWU2	0.005695(6)	4.54×10^6
13	70	0	2010/155/04	2010/158/04	NWU2	0.005756(15)	6.45×10^5
15	55	0	2010/162/07	2010/179/02	BRI	0.005007(2)	4.48×10^6

[a]For Configurations 1–13, the calibrator was outside the PSNM building as in Figure 3. For Configuration 15, the calibrator was inside the PSNM building as in Figure 2.
[b]Year/day of year/hour (UT).
[c]Calibrator to PSNM count rate ratio. Parentheses indicate statistical standard error in the final digits.
[d]Counts detected by the calibrator during usable times.

3. Data Analysis

3.1. Calibrator Data

Operating in the outdoor location with tropical heat and humidity posed technical challenges for the electronics. Fortunately, the NWU1 and NWU2 electronics recorded data with a cadence of 1 s, allowing individual seconds to be rejected as necessary. While the standard count rate was 3.5 Hz, the NWU1 electronics recorded 1 to 2 s of noise (> 10 counts) with a period of about 10 s, especially during time periods with direct sunlight. Therefore, an individual 1 s record was rejected if there were > 10 counts in that record and also in a record 9, 10, or 11 s earlier or later. A record was also rejected if the recorded counter temperature was outside the range of 0 to 40°C, apparently due to a readout error, which typically occurred in occasional pairs of adjacent seconds for which the voltage readout was also abnormal. During some hours, typically during daytime, up to 20% of the records were rejected for these reasons. For the various configurations, an average of 7 to 14% of 1 s records was rejected. For the NWU2 electronics, the noise period was about 5 s, and the same rejection logic could be applied. For these configurations, an average of 31 to 40% of 1 s records was rejected. While the hourly Cal/NM ratio was extracted for both the NWU1 and NWU2 electronics, the NWU2 data are considered to be less reliable and were not further analyzed. The hourly ratio for these electronics was corrected for the temperature of the counter tube (not the temperature of the electronics), which varied over 10 to 30°C. The data were corrected to remove a positive correlation with temperature of 0.04% °C^{-1} as inferred in previous work [*Krüger and Moraal*, 2010], correcting to a standard counter temperature of 24°C.

The BRI electronics were designed for indoor use, but nevertheless, we made use of them in the outdoor conditions, including the extreme sunlight at mountain altitude. Because the standard count rate (CT) output did not function properly for an electronics temperature $T > 25$°C, which occurred frequently, we instead used the hourly pulse height (PH) output. The BRI CT rate (when available) was a few percent higher than the comparable NWU rates, and the PH rate was 23% lower than the CT rate, presumably because PH data have a much longer electronic dead time of 100 ± 1 μs. At some times $T > 60$°C was measured in the electronics head, and the PH data were affected by noise (typically) for electronics temperature $T > 40$°C and for 2 h afterward. Data were cut when a separate noise channel ("unselected" or U count rate) registered $U > 7000$ h^{-1}. This problem did not arise for observations with the calibrator inside the building. For usable data from the BRI electronics, we did not find a significant correlation of the Cal/NM ratio with counter temperature and did not perform a temperature correction.

For all configurations listed in Table 1, the Cal/NM ratio was determined for each hour of usable data, and these were used to determine the average value and uncertainty (standard error) of the ratio for each configuration. All configurations were outdoors (as in Figure 3), except for Configuration 15, for which the calibrator was inside the PSNM building (as in Figure 2). Results for the three sets of electronics can be directly compared for configurations 8 to 10, for which data were taken in succession with no changes to the calibrator height and water height. In particular, configurations 9 and 10 were for the same electronics with a different preamplifier (NWU1 and NWU2) and those Cal/NM values differed by 2.4%, compared with a maximum standard error of 0.1% for individual measurements. We found only a marginally significant effect of atmospheric pressure on the Cal/NM ratio; i.e., the calibrator and PSNM have almost the same barometric coefficient to within measurement uncertainty. In our analysis the Cal/NM ratio has not been corrected for atmospheric pressure; we discuss the issue further in sections 3.3 and 5.

3.2. Effect of Surrounding Structure

Observations of the effects of the calibrator height and water height at Doi Inthanon, as well as the calibration result, have been previously reported [*Krüger et al.*, 2011]. The effect of water is to moderate neutrons, and the Cal/NM ratio decreases with increasing water height, as expected. As previously reported by *Krüger et al.* [2011], this is consistent with prior measurements with a calibrator at Kiel, Germany, and Potchefstroom, South Africa [*Krüger and Moraal*, 2010].

To measure the effect of the PSNM building on the count rate ratio, we compared data for Configuration 8, with the calibrator outdoors at a calibrator height of 70 cm and water height of 65 cm as recommended for calibration purposes [*Krüger and Moraal*, 2010], with those from Configuration 15, with the calibrator inside the building with no water underneath (see Table 2). For these two configurations, we collected 9.1×10^6 and 4.5×10^6 counts, respectively, and used the same (BRI) electronics, so we are able to precisely determine the small change in the Cal/NM ratio. This ratio was 0.004860(2) outside the building and 0.005007(2) inside. We will discuss the reasons for this difference (about 3%) in sections 4.2 and 5.

Table 2. Observational and Simulation Results for Calibrator Outside and Inside the Building[a]

	Calibrator		PSNM
	Outside	Inside	
Observed hourly count rate for calibrator outside[b]	10,674(6)	—	$2.1964(9) \times 10^6$
Observed hourly count rate for calibrator inside[c]	—	11,160(7)	$2.2289(10) \times 10^6$
Observed count rate, relative to PSNM	$4.860(2) \times 10^{-3}$	$5.007(2) \times 10^{-3}$	1
Monte Carlo hourly count rate	12,148(75)	13,126(143)	$2.502(2) \times 10^6$
Monte Carlo count rate, relative to PSNM	$4.86(3) \times 10^{-3}$	$5.25(6) \times 10^{-3}$	1

[a]Parentheses indicate statistical standard error in the final digits. All count rates are uncorrected.
[b]Configuration 8, during 11 February to 6 April 2010.
[c]Configuration 15, during 11–28 June 2010.

3.3. Atmospheric Effects

We have investigated a possible dependence of the Cal/NM ratio on atmospheric pressure, p, as measured using barometers on site, and atmospheric water vapor pressure, E_w. The latter was determined using the Global Data Assimilation System (GDAS) database, which is available from http://ready.arl.noaa.gov/gdas1.php. We downloaded the values of relative humidity H and temperature T from the GDAS database for a pressure level of 750 hPa at the four surrounding spatial grid points and interpolated H and T to the geographic location of PSNM. We then used the formula

$$E_w = (6.113 \text{ hPa}) \frac{H}{100} \exp\left(\frac{17.62\,T}{T + 243.12}\right) \tag{1}$$

where H is expressed in percent and T in degrees Celsius.

The measurement with the calibrator outside spanned the months of February to April, during the dry season, with mean values $p_o = 752.48$ hPa and $E_{wo} = 6.9$ hPa. The measurement with the calibrator inside was performed in June, during the rainy season, with mean values $p_i = 749.50$ hPa and $E_{wi} = 13.7$ hPa. Because Configuration 8 lasted for a longer time with much greater variability in atmospheric conditions, we used data from that time period to perform a linear regression of the Cal/NM ratio with either p or E_w, obtaining regression coefficients of $-(1.58 \pm 1.13) \times 10^{-6}$ hPa^{-1} and $(1.41 \pm 1.19) \times 10^{-6}$ hPa^{-1}, respectively, both of which are marginally significant. Multiplying with the differences in p and E_w between inside and outside, these trends would make the Cal/NM ratio inside lower by $(10.7 \pm 7.7) \times 10^{-6}$ and $(4.2 \pm 3.6) \times 10^{-6}$, respectively. We note that in both cases, visual inspection of the time series does not reveal an obvious association between variations in the Cal/NM ratio and either atmospheric variable, so we consider that these effects are not well determined. Therefore, we do not correct for these possible atmospheric effects and consider that they represent an uncertainty in the results. The uncertainty is minor compared with the difference in the Cal/NM ratio outside and inside (the Cal/NM ratio inside is higher by $(1.47 \pm 0.03) \times 10^{-4}$), but it is relevant to the accuracy of the calibration, as will be discussed in section 5.

4. Monte Carlo Simulations

4.1. Methods

To model the yield functions of the 18NM64 and calibrator at Doi Inthanon, we have performed Monte Carlo simulations of (1) cosmic ray interactions in Earth's atmosphere to produce atmospheric secondary cosmic rays and (2) the interactions of those secondary particles in the neutron monitors and their surrounding structure. Following *Clem and Dorman* [2000], we used the FLUKA 2011.2b-5 simulation package [*Ferrari et al.*, 2005; *Bohlen et al.*, 2014]. The HEAVYNUC option was used with the interaction model DPMJET-2.5 as recommended in the FLUKA manual. The PHOTONUC option (for photonuclear processes) was fully activated, and the production of electromagnetic components was cut below 1 MeV for $e^{\pm}$ and below 100 keV for γ.

The primary GCR spectrum above the atmosphere was modeled from the local interstellar spectrum described in *Usoskin et al.* [2011]. A solar modulation parameter $\phi = 340$ MV was applied, which

corresponds to the mean value of the modulation parameter of the force field approximation [*Gleeson and Axford*, 1968] during the first 6 months of 2010. The atmosphere above Doi Inthanon was modeled using detailed GDAS data for the month of January in the dry season. Data were averaged from 2006 to 2013 throughout their altitude range, up to ∼26 km. Above that, we used the NRLMSISE-00 model (with only dry air) [*Picone et al.*, 2002], which is available at http://ccmc.gsfc.nasa.gov/modelweb/models/nrlmsise00.php. For the present runs, the total pressure and the water vapor pressure at Doi Inthanon were taken to be 751.1 hPa and 6.3 hPa, respectively, as appropriate for January.

In the first-stage (atmospheric) simulations, we modeled atmospheric showers caused by the primary particles in a spherical atmosphere. The primary particles were assumed to be isotropic in space, following *Clem et al.* [2004], and were simulated uniformly for several ranges of kinetic energy per nucleon. The simulation data were weighted in postsimulation processing to apply the desired primary GCR spectrum and to only select particles with an energy and arrival direction that allowed penetration of Earth's magnetic field. For such selection, we employed the techniques of *Lin et al.* [1995] to directly trace each individual simulated primary particle through the geomagnetic field using version 11 of the coefficients of the International Geomagnetic Reference Field 11. We collected data on a population of 3.05×10^7 secondary particles of various species at the altitude of Doi Inthanon. In the second stage, we considered either the PSNM station with calibrator and 18NM64 inside for Configuration 15 (as in Figure 2), or the calibrator outside for Configuration 8 (Figure 3). Secondary particles were randomly chosen from the population generated in the first-stage simulation and started at initial positions uniformly randomized over a horizontal rectangular region (to be described below), and we followed their interactions through all materials in the simulation region. Whenever a neutron entered a counter tube, whether the neutron was a secondary particle or (more commonly) produced by interactions of secondary particles in local materials, we counted neutron interactions with ^{10}B or ^3He in the counter tubes of the 18NM64 or calibrator, respectively. Combining results from the first and second stages, we determined the count rates expected in the 18NM64 and calibrator inside the PSNM station or the calibrator outside the station.

We made a special effort to develop an appropriate beam pattern for secondary particles moving toward the detectors. The particles in the beam were initially distributed randomly over a horizontal rectangle defined by a constant height above ground level and a rectangle size that depended on the particle incidence angle. The initial height was a short distance above all structures, at 6 m above the floor (for inside runs) or 5.4 m above the ground, which was 2.32 m above the calibrator center (for outside runs). All secondary particles were simulated starting at this initial height. Secondary particles moving vertically downward were initially randomized over a minimum-size, horizontal rectangle, designed to be wide enough to illuminate all surrounding structure and part of the surrounding concrete or ground. The minimum-size rectangle had dimensions 15 m × 17 m (inside) or 3.8 m × 4.4 m (outside), with sides parallel to the walls of the building or bunker. For other initial directions (downward, but, in general, nonvertical), the initial rectangle was designed to encompass the minimum rectangle but was stretched so that the beam would completely illuminate the projection of the minimum rectangle vertically down to the ground. The output was then weighted according to the incidence angle to compensate for the change in number of particles per unit horizontal area of the initial rectangle (beam luminosity). In this way, a different initial horizontal rectangle was used for different initial directions, with a size large enough to encompass the detectors and surroundings.

We performed the Monte Carlo simulations on a Linux cluster of 30 nodes and 120 CPUs. The first-stage Monte Carlo runs required about 5 days. The second-stage Monte Carlo runs were performed in cycles of 10^7 particles each. For inside runs the run time was 23.4 CPU hours per cycle, and for outside runs the time was 7.1 CPU hours per cycle. We used about 1300 cycles for the 18NM64 and the calibrator inside and 1400 cycles for the calibrator outside.

4.2. Results

In postprocessing of the Monte Carlo simulation results, we applied an electronic dead time t_d to reject events arriving within t_d of a recorded event. We found that for each detector, increasing the dead time causes the count rate to decrease significantly (Figure 4). The decrease is stronger in the calibrator, presumably because it uses a ^3He tube, which has greater counting efficiency so there is typically a shorter delay between successive neutrons from the same interaction. The effect of the dead time is even found to be different for the calibrator inside or outside, indicating that this effect contributes to a detector's sensitivity to its environment.
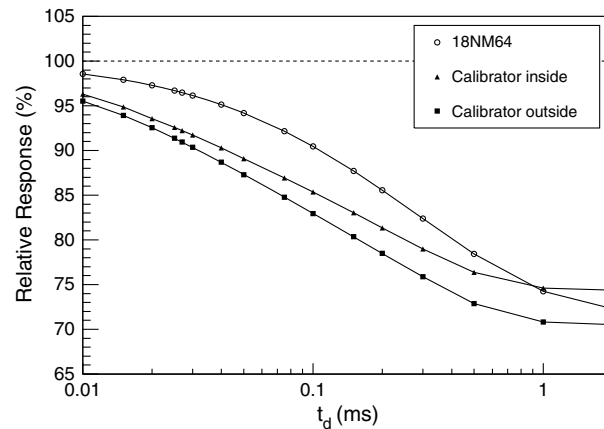
Figure 4. Monte Carlo results for the dependence of count rate on dead time for the 18NM64 and the calibrator inside and outside, relative to zero dead time. Subsequent Monte Carlo results make use of the measured dead times of the 18NM64 tubes (ranging from 18 to 29 μs) and of the calibrator pulse height rates (100 μs).

Note that the accuracy goal of the 18NM64 at Doi Inthanon is 0.1%, and the calibration accuracy goal is 0.2%, so even a minor change in the dead time has a quite important effect on the count rate. Fortunately, the electronic dead time seems to be constant in time for a given set of electronics, so the dead time may not affect the stability of the count rate from a fixed station. For the calibrator, the calibration procedure requires comparing the count rate with another calibrator at a reference location, so the variability between different electronics units is relevant as is the dependence on surrounding structure.

The effect of dead time on the count rate N is closely related to the distribution of time delays between one neutron count and the next [*Bieber et al.*, 2004]. More specifically, $-dN/dt_d$ is related to the probability of a time delay equal to t_d. In Figure 4, for $t_d > 1$ ms the calibrator count rates are nearly constant with t_d, while that of the 18NM64 continues to decline. This is because each 18NM64 tube has a higher count rate (≈ 34 Hz) and thus a higher probability of a chance coincidence with a time delay of ~ 1 ms, compared with the calibrator with a count rate of ≈ 3.5 Hz.

As mentioned earlier, for technical reasons Configurations 8 and 15 used the PH count rate of the BRI electronics. These electronics recorded time delay histograms, so we can measure the dead time for the PH rate as 100 ± 1 μs. For the 18NM64, which also has BRI electronics but uses the CT count rate, we have measured the dead time for each tube, and the values range from 18 to 29 μs. For subsequent Monte Carlo results, we have applied the appropriate dead time for each tube in postprocessing.

Table 2 shows the results of observations and Monte Carlo simulations for Configuration 8 (outside) and Configuration 15 (inside). The Monte Carlo results for the Cal/NM ratio agree with observations to within a few percent. For the absolute count rates, the Monte Carlo results are high by 13% to 18%. This could be predominantly due to uncertainty in the chosen primary GCR spectrum. According to *Herbst et al.* [2010], different published parameterizations of the local interstellar spectrum lead to estimates of the GCR proton flux at 20 GeV near Earth that differ by up to ~10% when normalized to data from the PAMELA instrument, and PAMELA data themselves are uncertain to ~5% [*Adriani et al.*, 2013].

In addition, there are other possible reasons why the Monte Carlo results for absolute count rates differ from observations by 13 to 18%. The Monte Carlo results depend on the hadron interaction model and the assumed atmospheric profile [*Bernlöhr*, 2000; *Keilhauer et al.*, 2004; *Mishev and Velinov*, 2014].

Note that the difference in PSNM count rates for the calibrator outside and inside is mainly due to a change in atmospheric pressure between the two time periods (see section 3.3). When correcting using PSNM's standard pressure coefficient of 0.6406% hPa^{-1} to its standard pressure of 750.6 hPa, the PSNM hourly count rates become $2.2230(9) \times 10^6$ and $2.2132(10) \times 10^6$ when the calibrator was outside and inside, respectively. The remaining variability is associated with temporal changes in the primary GCR flux.

The observations and Monte Carlo results agree that the Cal/NM ratio was higher when the calibrator was inside the building. To gain more insight into this result, we used Monte Carlo simulations to estimate the contributions of various secondary species to the count rates of PSNM and the calibrator outside and inside. Table 3 gives the total contribution of each species, including neutrons in three energy ranges, as a percentage of the count rate in each detector. For the PSNM, which has 18 tubes in the standard NM64 design (i.e., 18NM64), secondary neutrons account for $\approx 80\%$ of the count rate, followed by protons (15%), muons (2%), photons (1%), and other species.

Table 3. Percentage Contributions of Various Cosmic Ray Shower Components to Neutron Monitor Count Rates in Monte Carlo Simulations[a]

	Calibrator		
	Outside	Inside	PSNM
$n, E_k < 10$ MeV	6.5(1)	6.2(2)	1.460(6)
$n, 10$ MeV $\leq E_k < 1$ GeV	69.2(2)	68.8(4)	63.10(4)
$n, E_k \geq 1$ GeV	8.57(9)	9.3(2)	15.68(3)
p	10.5(1)	10.7(2)	15.31(3)
γ	2.20(3)	1.89(7)	1.213(4)
μ^-	1.74(3)	1.81(8)	1.871(6)
μ^+	0.25(1)	0.23(2)	0.321(3)
π^-	0.193(9)	0.22(3)	0.333(4)
π^+	0.163(9)	0.16(2)	0.291(4)
e^-	0.40(1)	0.39(3)	0.221(2)
e^+	0.38(1)	0.31(3)	0.202(2)

[a]Parentheses indicate statistical standard error in the final digits.

The percentages shown in Table 3 are substantially different for the calibrator, and there are even differences between the calibrator outside and inside. To better understand these differences, Figure 5 gives absolute (unnormalized) count rates in Hertz per kinetic energy bin for the calibrator outside and the 18NM64 inside associated with nine species of secondary particles. In each panel, the vertical scales for the two detectors differ by a factor of 200, which roughly corresponds to the overall count rate ratio. Note that this factor is equal to the ratio of lead producer mass (29 t for the 18NM64 versus 145 kg for the calibrator).

Some features in Figure 5 are common to both detectors. Their count rates are dominated by n of 10 MeV to 10 GeV, followed by p of 100 MeV to 100 GeV. The count rate due to secondary γ exhibits a sharp peak in the energy bin below 20 MeV, corresponding to the giant dipole resonance in lead. The $\mu^\pm$ responses have peaks of similar magnitude just below 10 GeV, but in addition, the μ^- response has a much larger peak above 100 MeV corresponding to the formation of muonic atoms. In the case of lead, the μ^- can enter an orbital that is largely inside the nucleus, leading to an enhanced probability of disrupting the nucleus and producing evaporation neutrons that are subsequently detected in the neutron counters. This effect makes μ^- the third most detected species in the 18NM64. For the minor secondary species $\pi^\pm$ and $e^\pm$, the count rate is dominated by secondary particles of ~1 GeV.

Compared with the 18NM64, the calibrator is relatively less sensitive to charged hadrons (p, $\pi^\pm$) and more sensitive to electromagnetic components (γ, $e^\pm$). Indeed, for the calibrator (outside or inside), γ replaces μ^- as the third most detected secondary species. The overall responses to n and $\mu^\pm$ remain roughly similar. However, Table 3 and Figure 5 indicate that the calibrator is much more sensitive to n with 0.5 MeV $< E_k <$ 10 MeV. This can help account for the environmental sensitivity that we observe with the calibrator, which will be discussed further in section 5. Furthermore, in the main peaks of energy sensitivity, the 18NM64 sensitivity is shifted to higher energy for n, p, $\mu^\pm$, and $\pi^\pm$. This may be largely due to the building structure above the 18NM64, which serves as an additional producer that enhances the contribution of more energetic secondary particles.

Our Monte Carlo simulations are also able to discern a difference between the responses of the calibrator outside versus inside the PSNM building. Figure 6 shows the count rates due to secondary n and p of various energies, which are systematically different for the calibrator outside and inside. The peaks for both species are shifted to higher energy when the detector is inside the building, which is qualitatively consistent with the shift for the 18NM64 inside relative to the calibrator outside as seen in Figure 5. For other secondary particle species, the differences in count rate versus particle energy for the calibrator outside and inside are dominated by Monte Carlo statistical fluctuations, though according to Table 3 the overall γ distribution is significantly higher for the calibrator outside.
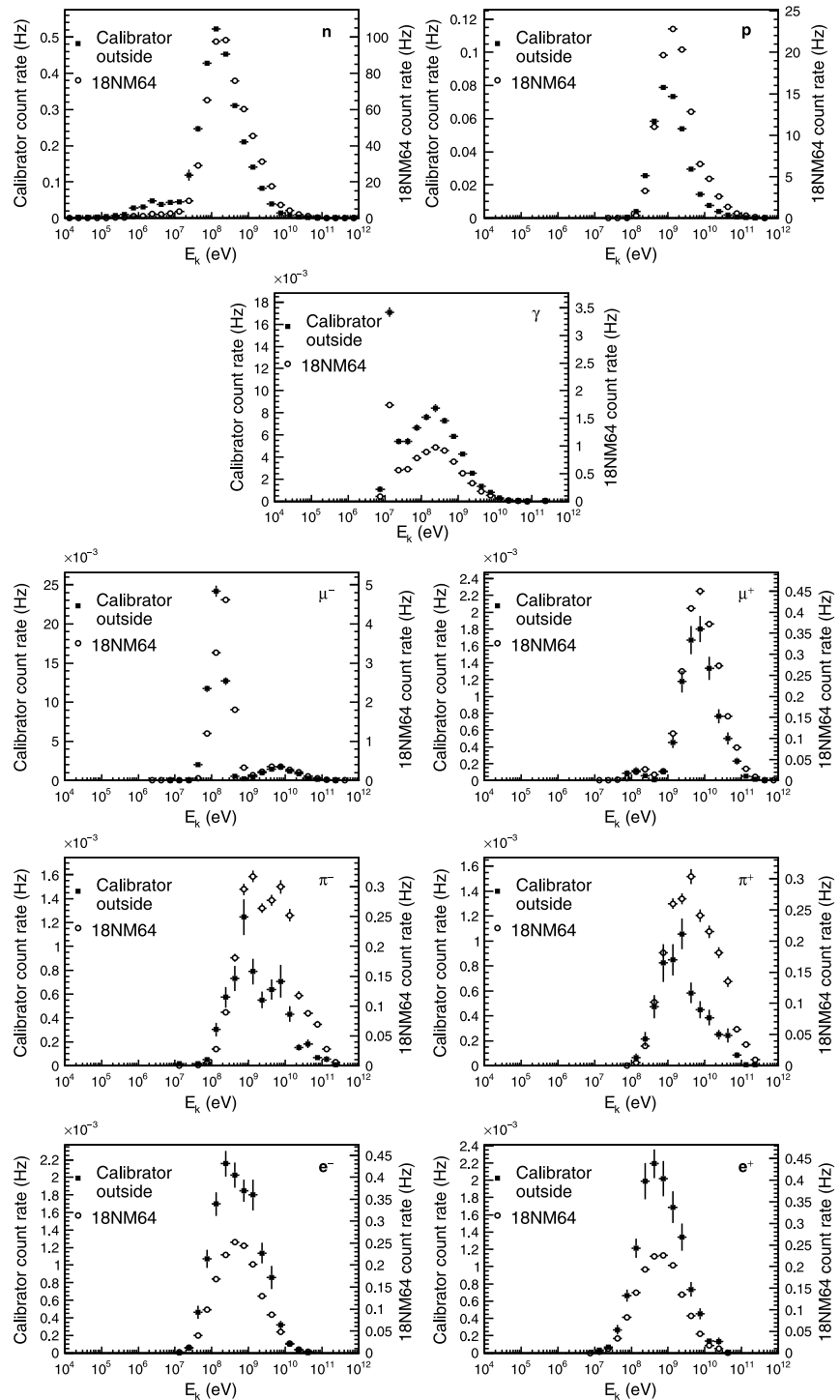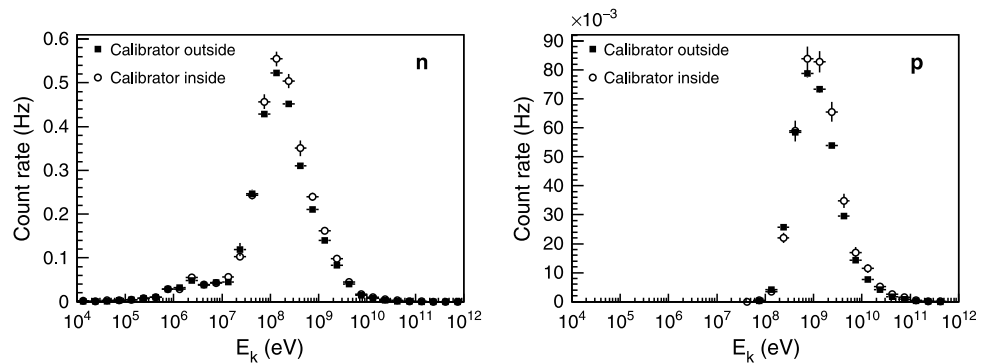
Figure 5. Simulated neutron monitor count rates produced by various types of atmospheric secondary cosmic rays arriving to ground level within specific bins of kinetic energy, for the calibrator outside the PSNM building (Configuration 8; solid circles) and the 18-tube NM64 detector inside (open circles), according to Monte Carlo simulations. In each plot, the scales used for the two detectors differ by a factor of 200, approximately corresponding to the overall count rate ratio. The 18NM64 is more sensitive to n of $E > 200$ MeV, while the calibrator is much more sensitive to those with 0.5 MeV $< E <$ 10 MeV, which are mainly produced by secondary cosmic ray interactions in the environment at ground level. The energy range of 18NM64 sensitivity is also noticeably shifted to higher E for p, $\mu^\pm$, and $\pi^\pm$. The calibrator is relatively less sensitive to charged hadrons and more sensitive to electromagnetic components.

Figure 6. Simulated neutron monitor count rates produced by various types of atmospheric secondary cosmic rays arriving to ground level within specific bins of kinetic energy, for the calibrator outside the PSNM building (Configuration 8; solid circles) and inside (Configuration 15; open circles), according to Monte Carlo simulations, which are sufficiently accurate to show differences in the response to these species according to the surrounding structure. The simulations show overall higher count rate for the calibrator inside, as in our observations. Furthermore, the simulations indicate that the response was shifted to higher energies when the calibrator was inside the building, suggesting an effect of the surrounding structure on the spectral response to cosmic rays.

5. Discussion and Conclusions

A portable calibration neutron monitor ("calibrator") was operated in concert with the Princess Sirindhorn Neutron Monitor (PSNM) at Doi Inthanon, Thailand. This experiment is part of a calibration of the world's neutron monitors, with a target accuracy of 0.2%. The analysis of data from the calibrator and PSNM, together with Monte Carlo simulations, revealed the following challenges regarding the calibration concept and its target accuracy.

1. *Electronics.* Operating the calibrator with different electronics units, or even different forms of output from the same unit, yielded substantially different Cal/NM count rate ratios (see Table 1). Even for the same physical configuration and electronics except for a different preamplifier (i.e., Configurations 9 and 10 with the NWU1 and NWU2 electronics, respectively), the Cal/NM ratio was different by 2.4%. Since the calibration concept requires comparing contemporaneous data from two different calibrator units in different parts of the world [*Krüger et al.*, 2011], the uncertainty from using different units of the same type of electronics is directly relevant. When operating in the harsh sunlight at mountain altitude, there were numerous time periods of noisy output. The count rate was found to depend on the discriminator thresholds, perhaps due to the presence of noise. According to our observations and Monte Carlo simulations, the count rate from the calibrator's ^{3}He counter tube is also very sensitive to the dead time. For all outdoor configurations and all sets of electronics, after removing electronic noise as best we could, the Cal/NM ratio still drifted upward and downward in time.

2. *Possible seasonal effects.* We cannot determine conclusively whether the Cal/NM ratio depends on atmospheric properties that vary with the season (e.g., rainy season versus dry season), such as atmospheric water vapor content and barometric pressure. As described in section 3.3, our best estimate of such effects on the Cal/NM ratio from the time of Configuration 8 to that of Configuration 15 at Doi Inthanon is $(-1.5 \pm 0.8) \times 10^{-5}$, or a change of (-0.3 ± 0.2)%. This implies that a calibration during one season may not apply to all seasons within the accuracy goal.

3. *Unknown pressure correction from mountain altitude.* Even if the Cal/NM ratio depends on pressure at a level that is too small to measure clearly at a fixed location, where the pressure varies only by several hectopascals, the calibration concept compares such ratios at mountain altitude and near sea level, i.e., over a range of ∼260 hPa. Our best estimate of the pressure coefficient of the ratio, when extrapolated to a pressure change of +260 hPa, implies a Cal/NM increase by (8 ± 7)%. This may represent the greatest uncertainty in the worldwide calibration effort.

4. *Solar modulation.* Even if a calibration at one epoch is accurate to within 0.2%, given the different responses to secondary cosmic rays of the calibrator and 18NM64, there is some uncertainty as to whether the Cal/NM ratio varies with the change in the cosmic ray spectrum from solar minimum to solar maximum.

5. *Local environment.* The use of a pool of water greatly helps to provide a standard environment for calibration in different locations. Despite this, there are possible effects on the Cal/NM ratio from other aspects of the

environment, such as the support structure under the calibrator (in our case, four concrete legs), rainwater, distance of the pool above the ground, and characteristics of the ground.

In addition to the calibration program, we found the calibrator data to be quite useful for observing the effect of surrounding structure on a neutron monitor count rate, and for validating Monte Carlo simulations to within a few percent. The ultimate solution for properly interpreting neutron monitor count rates and combining them to monitor the cosmic ray spectrum may be to use Monte Carlo simulations to estimate effects such as these on neutron monitor yield functions.

Our Monte Carlo simulations already shed light on the dependence of the calibrator count rate on its environment (this dependence was also reported by *Krüger and Moraal* [2010] and *Krüger et al.* [2011]). Referring to Table 3 and Figure 5, the calibrator is much more sensitive to n of $E_k < 10$ MeV. To understand the environmental sensitivity of these detectors, note that the 18NM64 is mostly sensitive to secondary n and p of $E_k \geq 10$ MeV that directly penetrate the building and polyethylene reflector to interact in the lead, causing evaporation neutrons from the lead nucleus to be detected in the counters. These high-energy secondary cosmic rays are affected by atmospheric conditions but are rather insensitive to local conditions, except for the amount of matter they encounter on the way down. That should remain constant at a fixed station, except for stations that accumulate snow cover, which is not the case at Doi Inthanon. In contrast, n of $E_k < 10$ MeV are more likely to be products of secondary cosmic ray interactions near the surface, which makes their flux more sensitive to local temperature, rainwater on the ground, etc. Indeed, bare counters without a lead producer are widely used to detect soil moisture [e.g., *Zreda et al.*, 2008], because water can strongly moderate such low-energy neutrons. While the calibrator is nowhere near as sensitive to low-energy environmental neutrons as a bare counter is, it is more sensitive than the 18NM64, perhaps because the calibrator reflector endcaps are thinner (50 mm) than the reflector surrounding the 18NM64 (76 mm). This can explain our observations that the calibrator count rate decreases with increased water height (e.g., for Configurations 1–4 in Table 1) and increases when placed inside the PSNM station, surrounded by more neutron-producing materials.

In summary, we deployed a portable calibration neutron monitor (calibrator) to Doi Inthanon, Thailand, for operation in conjunction with the Princess Sirindhorn Neutron Monitor (PSNM). This calibration run also provided a special opportunity to measure the sensitivity of the calibrator to its environment and determine the effect on the Cal/NM count rate ratio of placing the calibrator outside and inside the PSNM building. We performed detailed Monte Carlo simulations of atmospheric showers caused by galactic cosmic rays, and the interactions of secondary shower particles in the detectors and their surrounding structure. We found that the electronic dead time has a significant effect on the count rate, which is different for different types of detectors or even for the calibrator in different locations. Detectors located inside the building have a response that is shifted to higher energies for neutrons and several other species, and the calibrator has enhanced sensitivity to environmental neutrons of 0.5–10 MeV. These effects can explain its count rate dependence on surrounding structure. Monte Carlo simulation results matched observations of the Cal/NM ratio to within a few percent, both outside and inside the building, providing validation of our ability to model the yield functions of neutron monitors.

References

Adriani, O., et al. (2013), Time dependence of the proton flux measured by PAMELA during the 2006 July–2009 December solar minimum, *Astrophys. J.*, *765*, 91, doi:10.1088/0004-637X/765/2/91.

Bernlöhr, K. (2000), Impact of atmospheric parameters on the atmospheric Cherenkov technique, *Astropart. Phys.*, *12*, 255–268, doi:10.1016/S0927-6505(99)00093-6.

Bieber, J. W., J. M. Clem, M. L. Duldig, P. A. Evenson, J. E. Humble, and R. Pyle (2004), Latitude survey observations of neutron monitor multiplicity, *J. Geophys. Res.*, *109*, A12106, doi:10.1029/2004JA010493.

Bohlen, T. T., F. Cerutti, M. P. W. Chin, A. Fassò, A. Ferrari, P. G. Ortega, A. Mairani, P. R. Sala, G. Smirnov, and V. Vlachoudis (2014), The FLUKA code: Developments and challenges for high energy and medical applications, *Nucl. Data Sheets*, *120*, 211–214.

Caballero-Lopez, R. A., and H. Moraal (2012), Cosmic-ray yield and response functions in the atmosphere, *J. Geophys. Res.*, *117*, A12103, doi:10.1029/2012JA017794.

Clem, J. M., and L. I. Dorman (2000), Neutron monitor response functions, *Space Sci. Rev.*, *93*, 335–359, doi:10.1023/A:1026508915269.

Clem, J. M., G. De Angelis, P. Goldhagen, and J. W. Wilson (2004), New calculations of the atmospheric cosmic radiation field—Results for neutron spectra, *Radiat. Prot. Dosim.*, *110*, 423–428.

Cramp, J. L., M. L. Duldig, E. O. Flückiger, J. E. Humble, M. A. Shea, and D. F. Smart (1997), The October 22, 1989, solar cosmic ray enhancement: An analysis of the anisotropy and spectral characteristics, *J. Geophys. Res.*, *102*, 24,237–24,248, doi:10.1029/97JA01947.

Ferrari, A., P. R. Sala, A. Fassò, and J. Ranft (2005), *FLUKA: A Multi-Particle Transport Code*, CERN, Geneva. Report CERN-2005-10.

Gleeson, L. J., and W. I. Axford (1968), Solar modulation of galactic cosmic rays, *Astrophys. J.*, *154*, 1011–1026, doi:10.1086/149822.

Grieder, P. K. F. (2001), *Cosmic Rays at Earth*, Elsevier, Amsterdam.

Hatton, C. J., and H. Carmichael (1964), Experimental investigation of the NM-64 neutron monitor, *Can. J. Phys.*, *42*, 2443–2472, doi:10.1139/p64-222.

Herbst, K., A. Kopp, B. Heber, F. Steinhilber, H. Fichtner, K. Scherer, and D. Matthiä (2010), On the importance of the local interstellar spectrum for the solar modulation parameter, *J. Geophys. Res.*, *115*, D00I20, doi:10.1029/2009JD012557.

Keilhauer, B., J. Blümer, R. Engel, H. O. Klages, and M. Risse (2004), Impact of varying atmospheric profiles on extensive air shower observation: Atmospheric density and primary mass reconstruction, *Astropart. Phys.*, *22*, 249–261, doi:10.1016/j.astropartphys.2004.08.004.

Krüger, H., and H. Moraal (2010), A calibration neutron monitor: Statistical accuracy and environmental sensitivity, *Adv. Space Res.*, *46*, 1394–1399, doi:10.1016/j.asr.2010.07.008.

Krüger, H., H. Moraal, J. W. Bieber, J. M. Clem, P. A. Evenson, K. R. Pyle, M. L. Duldig, and J. E. Humble (2003), First results of a mobile neutron monitor to intercalibrate the worldwide network, paper presented at 28th International Cosmic Ray Conference, IUPAP, Tsukuba, Japan, vol. 6, 3441–3444.

Krüger, H., H. Moraal, J. W. Bieber, J. M. Clem, P. A. Evenson, K. R. Pyle, M. L. Duldig, and J. E. Humble (2008), A calibration neutron monitor: Energy response and instrumental temperature sensitivity, *J. Geophys. Res.*, *113*, A08101, doi:10.1029/2008JA013229.

Krüger, H., H. Moraal, D. Ruffolo, A. Sáiz, T. Nutaro, N. Kamyan, W. Nuntiyakul, B. Heber, and C. Steigies (2011), Progress report on the intercalibration of the world's neutron monitors, paper presented at 32nd International Cosmic Ray Conference, IUPAP, Beijing, China, vol. 11, 451–454, doi:10.7529/ICRC2011/V11/0436.

Lin, Z., J. W. Bieber, and P. Evenson (1995), Electron trajectories in a model magnetosphere: Simulation and observation under active conditions, *J. Geophys. Res.*, *100*, 23,543–23,550, doi:10.1029/95JA02696.

Mewaldt, R. A., et al. (2010), Record-setting cosmic-ray intensities in 2009 and 2010, *Astrophys. J. Lett.*, *723*, L1–L6, doi:10.1088/2041-8205/723/1/L1.

Mishev, A. L., and P. I. Y. Velinov (2014), Influence of hadron and atmospheric models on computation of cosmic ray ionization in the atmosphere—Extension to heavy nuclei, *J. Atmos. Sol. Terr. Phys.*, *120*, 111–120, doi:10.1016/j.jastp.2014.09.007.

Mishev, A. L., I. G. Usoskin, and G. A. Kovaltsov (2013), Neutron monitor yield function: New improved computations, *J. Geophys. Res. Space Physics*, *118*, 2783–2788, doi:10.1002/jgra.50325.

Moraal, H., A. Belov, and J. M. Clem (2000), Design and co-ordination of multi-station international neutron monitor networks, *Space Sci. Rev.*, *93*, 283–303, doi:10.1023/A:1026504814360.

Moraal, H., H. Krüger, A. Benadie, and D. de Villiers (2003), Calibration of the Sanae and Hermanus neutron monitors, paper presented at 28th International Cosmic Ray Conference, IUPAP, Tsukuba, Japan, vol. 6, 3453–3456.

Nuntiyakul, W., P. Evenson, D. Ruffolo, A. Sáiz, J. W. Bieber, J. Clem, R. Pyle, M. L. Duldig, and J. E. Humble (2014), Latitude survey investigation of galactic cosmic ray solar modulation during 1994–2007, *Astrophys. J.*, *795*, 11, doi:10.1088/0004-637X/795/1/11.

Okazaki, Y., et al. (2008), Drift effects and the cosmic ray density gradient in a solar rotation period: First observation with the Global Muon Detector Network (GMDN), *Astrophys. J.*, *681*, 693–707, doi:10.1086/588277.

Picone, J. M., A. E. Hedin, D. P. Drob, and A. C. Aikin (2002), NRLMSISE-00 empirical model of the atmosphere: Statistical comparisons and scientific issues, *J. Geophys. Res.*, *107*(A12), 1468, doi:10.1029/2002JA009430.

Usoskin, I. G., G. A. Bazilevskaya, and G. A. Kovaltsov (2011), Solar modulation parameter for cosmic rays since 1936 reconstructed from ground-based neutron monitors and ionization chambers, *J. Geophys. Res.*, *116*, A02104, doi:10.1029/2010JA016105.

Vashenyuk, E. V., Yu. V. Balabin, J. Perez-Peraza, A. Gallegos-Cruz, and L. I. Miroshnichenko (2006), Some features of the sources of relativistic particles at the Sun in the solar cycles 21–23, *Adv. Space Res.*, *38*, 411–417, doi:10.1016/j.asr.2005.05.012.

Yeeram, T., D. Ruffolo, A. Sáiz, N. Kamyan, and T. Nutaro (2014), Corotating solar wind structures and recurrent trains of enhanced diurnal variation in galactic cosmic rays, *Astrophys. J.*, *784*, 136, doi:10.1088/0004-637X/784/2/136.

Zreda, M., D. Desilets, T. P. A. Ferré, and R. L. Scott (2008), Measuring soil moisture content non-invasively at intermediate spatial scale using cosmic-ray neutrons, *Geophys. Res. Lett.*, *35*, L21402, doi:10.1029/2008GL035655.